Evaluation of Next-Generation Anti-CD20 Antibodies Labeled with ^{89}Zr in Human Lymphoma Xenografts

Jason T. Yoon*, Mark S. Longtine*, Bernadette V. Marquez-Nostra, and Richard L. Wahl

Mallinckrodt Institute of Radiology, Washington University, St. Louis, Missouri

Radioimmunotherapies with monoclonal antibodies to the B-lymphocyte antigen 20 (CD20) are effective treatments for B-cell lymphomas, but U.S. Food and Drug Administration–approved radioimmunotherapies exclusively use radiolabeled murine antibodies, potentially limiting redosing. The Food and Drug Administration recently approved 2 unlabeled anti-CD20 monoclonal antibodies, obinutuzumab and ofatumumab, termed next generation as they are humanized (obinutuzumab) or fully human (ofatumumab), thus potentially allowing a greater potential for redosing than with previous-generation anti-CD20 antibodies, including rituximab (chimeric) and tositumomab (murine), which contain more murine peptide sequences. We prepared ^{89}Zr-ofatumumab and ^{89}Zr-obinituzumab and assessed their tumor targeting by PET/CT imaging and their biodistribution in a preclinical mouse model with CD20 xenografts to determine whether these antibodies have potential as theranostics or for radioimmunotherapy. **Methods:** Obinutuzumab, ofatumumab, rituximab, tositumomab, and human IgG (as control) were radiolabeled with ^{89}Zr. Raji Burkitt lymphoma xenografts were established in severe combined immunodeficient mice. Mice with palpable tumors (n = 4–9) were injected with ^{89}Zr-obinutuzumab, ^{89}Zr-ofatumumab, ^{89}Zr-rituximab, ^{89}Zr-tositumomab, or ^{89}Zr-IgG, with small-animal PET/CT images acquired at 1, 3, and 7 d after injection, and then sacrificed for biodistribution analyses. **Results:** At 1, 3, and 7 d after injection, all anti-CD20 antibodies showed clear tumor uptake on PET/CT, with minimal tumor uptake of IgG. Biodistribution data showed significantly ($P < 0.005$) higher tumor uptake for obinutuzumab (41.4 ± 7.6 percentage injected dose [%ID]/g), ofatumumab (32.6 ± 17.5 %ID/g), rituximab (28.6 ± 7.6 %ID/g), and tositumomab (28.0 ± 6.5 %ID/g) than IgG (7.2 ± 1.2 %ID/g). Tositumomab had much higher splenic uptake (186.4 ± 49.7 %ID/g, $P < 0.001$) than the other antibodies. **Conclusion:** ^{89}Zr-labeled obinutuzumab and ofatumumab localized to tumor as well as or better than labeled rituximab and tositumomab, 2 monoclonal antibodies that have been used previously in B-cell lymphoma radioimmunotherapy, and both obinutuzumab and ofatumumab have the potential for repeated dosing.

Key Words: CD20; lymphoma; positron emission tomography; targeted antibodies

J Nucl Med 2018; 59:1219–1224
DOI: 10.2967/jnumed.117.203299

An estimated 20,000 patients died from non-Hodgkin lymphoma (NHL) in 2017 in the United States (*1*). B-cell NHLs constitute 85% of these cases, and 90% of B-cell lymphomas are B-lymphocyte antigen 20 (CD20)–positive (*2,3*). Although immunotherapies using anti-CD20 monoclonal antibodies (mAbs), including rituximab (Rituxan; Roche), have drastically improved patient outcomes, clinical resistance against unlabeled mAbs such as rituximab necessitates continued research, including different approaches to immunotherapy.

In radioimmunotherapy, mAbs are conjugated to a radioisotope to deliver antibody-targeted radiation to malignant cells. In some settings, a smaller radiotracer dose of the antibody can be given to quantify dosimetry or assay radiotracer uptake in tumor or lack of uptake in key structures. The radiotracer can be the same as the therapeutic, such as in the ^{131}I dosimetric and treatment regimens in the previously Food and Drug Administration-approved tositumomab–plus–^{131}I-tositumomab treatment regimen (*3–6*), or can differ, as in the use of ^{111}In-radiolabeled anti-CD20 antibodies for scanning followed by ^{90}Y anti-CD20 for therapy, such as in the rituximab-plus-ibritumomab regimens as initially deployed and Food and Drug Administration–approved. Such radiotracers followed by radiopharmaceutical therapies can be referred to as theranostic regimens.

Clinical trials have demonstrated the effectiveness of anti-CD20 radioimmunotherapy against NHL, both as an initial treatment and for advanced-stage patients who are refractory to other systemic therapies, such as rituximab (*7*). Two examples of anti-CD20 radioimmunotherapy that have been used in the United States are Zevalin (^{90}Y-labeled ibritumomab tiuxetan; Spectrum Pharmaceuticals (*8*)) and Bexxar (GlaxoSmithKline (*9*)). Bexxar, which is ^{131}I labeled to murine anti-CD20 mAb tositumomab, was a radioimmunotherapy effective against relapsed and refractory NHL, including those cases refractory to the standard "naked" anti-CD20 mAb treatment with rituximab. Although Bexxar is no longer available in the United States, ^{131}I-rituximab itself has been used as a radioimmunotherapy, principally in Australia (*10*).

Although tositumomab and rituximab are both the foundation of anti-CD20s radioimmunotherapies (although purely murine ibritumomab is the labeled component of the Zevalin therapy), they represent 2 different categories of anti-CD20 mAbs. Rituximab, a type I anti-CD20 mAb, promotes the formation of membrane lipid rafts, strongly activates complement-dependent cytotoxicity, and binds in a 2:1, mAb-to-antigen, stoichiometry (*2,11*). Tositumomab, a type II anti-CD20 mAb, does not aggregate lipid rafts, strongly activates homotypic adhesion, induces apoptosis instead of complement-dependent cytotoxicity, and binds antigen in a 1:1 stoichiometry (*2,11*).

Received Oct. 5, 2017; revision accepted Dec. 24, 2017.
For correspondence or reprints contact: Richard Wahl, Washington University School of Medicine, Department of Radiology, Campus Box 8131, 660 S. Euclid Ave., St. Louis, MO 63110.
E-mail: wahlr@wustl.edu
*Contributed equally to this work.
Published online Jan. 18, 2018.

Despite these differences, rituximab, ibritumomab, and tositumomab all contain considerable amounts of mouse protein. In fact, all anti-CD20 radioimmunotherapies use either purely murine mAbs, such as tositumomab, or chimeric antibodies, such as rituximab with or without purely murine ibritumomab, and U.S. Food and Drug Administration–approved radioimmunotherapies were approved for only single therapeutic doses because of the risk of human antimouse antibody generation and potential allergic reactions. Recently, however, the Food and Drug Administration has approved next-generation anti-CD20 antibodies that are humanized (where only the complementarity-determining regions remain murine) or fully human. Obinutuzumab (Gazyva; Roche) is a humanized type II (tositumomablike) mAb approved for relapsed or refractory follicular lymphoma and chronic lymphocytic leukemia and for previously untreated follicular lymphoma (*12*). Ofatumumab (Arzerra; Novartis) is a fully-human type I (rituximablike) mAb approved for chronic lymphocytic leukemia (*13*). Humanized and fully-human antibodies have lower immunogenicity than murine or chimeric antibodies, allowing for the potential for safe retreatments (*2,14*). Furthermore, ofatumumab has been shown to be more effective than rituximab (and effective with rituximab-resistant cells) in in vitro and human lymphoma xenograft models, with superior cytotoxic activity and B-cell depletion in lymphoid tissue (*15*). Similarly, compared with rituximab, obinutuzumab displays increased cytotoxicity in cellular assays, superior antitumor activity in a xenograft model, and improved B-cell depletion in lymphoid tissue in nonhuman primates (*16*).

The goal of the current study was to investigate whether obinutuzumab and ofatumumab are candidates for an anti-CD20 radioimmunotherapy regimen, using the PET imaging radioisotope ^{89}Zr to examine in vitro immunoreactivity and in vivo tumor uptake with small-animal PET/CT and tissue biodistribution studies. We assessed how they compare with the current standards, rituximab and tositumomab, as well as with control human IgG. The translational goal is to ultimately use ^{89}Zr-obinutuzumab or ^{89}Zr-ofatumumab for imaging in human lymphoma patients and as a roadmap for radioimmunotherapies that use higher-energy radioisotopes. Although the incidence of development of human antimouse antibodies in Zevalin treatments appears low (*8*), this issue undoubtedly will be further reduced with human or humanized anti-CD20 antibodies, increasing the potential for more than one treatment with radioimmunotherapy.

MATERIALS AND METHODS

Reagents and Cell Lines

Obinutuzumab and rituximab were from the Washington University clinical pharmacy. Ofatumumab and tositumomab were from the Johns Hopkins University clinical pharmacy. Human IgG was from Fisher Scientific (catalog no. 31154). p-SCN-Bn-deferoxamine (Dfo) was from Macrocyclics (catalog no. B-705). The Raji Burkitt lymphoma cell line was from the American Type Culture Collection.

^{89}Zr Production, Antibody Conjugation with Dfo, and Chelation of ^{89}Zr

^{89}Zr-oxalate was produced at Washington University via the Y-89 (p,n)^{89}Zr reaction on a CS-15 cyclotron (Cyclotron Corp.) and purified with an in-house automated module (*17*). The resulting ^{89}Zr-oxalate was produced with a specific activity of 8.1–15.4 GBq/μmol (220–418 mCi/μmol).

Antibody conjugation and radiolabeling were done as previously described (*18*). Briefly, antibodies were diluted with phosphate-buffered saline to 5 mg/mL and exchanged into 0.1 M sodium carbonate buffer (pH 9.0) using 40-kDa molecular-weight-cutoff size-exclusion spin columns (Fisher Scientific, catalog no. PI87667). Dfo was dissolved in dimethyl sulfoxide at 5 mg/mL and added to the antibody solution at Dfo-to-antibody molar ratios of 10:1, 5:1, or 2:1. After 60 min at 37°C, the Dfo-antibody conjugate was purified from unconjugated Dfo and exchanged into 1.0 M 4-(2-hydroxyethyl)-1-piperazineethanesulfonic acid buffer (pH 7.0) using spin columns, and the antibody concentration was determined by bicinchoninic acid assay (Fisher Scientific, catalog no. 23227). Dfo-antibody conjugates were radiolabeled with neutralized ^{89}Zr-oxalate at 370 kBq (10 μCi)/μg for 1 h at 37°C. After addition of diethylenetriaminepentaacetic acid (pH 7.0) to 5 mM for 10 min at 37°C, ^{89}Zr-antibodies were separated from free ^{89}Zr using phosphate-buffered saline and spin columns.

Instant Thin-Layer Chromatography and Fast Protein Liquid Chromatography

Instant thin-layer chromatography was performed on silica gel paper (catalog no. SGI0001, Agilent) using 50 mM diethylenetriaminepentaacetic acid (pH 7.0) as solvent. Antibody-bound and free ^{89}Zr were quantified using a BioScan AR200 radio–thin-layer chromatography imaging scanner. Fast protein liquid chromatography analyses (AKTA Explorer; GE Healthcare) used a Superose 10/300 column (GE Healthcare) running 50 mM sodium phosphate and 150 mM NaCl (pH 7.0) buffer, with an in-line ultraviolet detector and an in-line radiodetector (Lab-Logic).

In Vitro Serum Stability

^{89}Zr-labeled antibodies (1.7 MBq) were diluted 1:10 into 190 μL of human serum (Sigma, catalog no. H4522) and incubated at 37°C or 4°C. After 24, 48, 72, 120, and 168 h, aliquots were incubated for 5 min at 23°C in 10 mM diethylenetriaminepentaacetic acid, pH 7.0, and examined by instant thin-layer chromatography.

Animal Studies

Animal studies were approved by the Washington University Institutional Animal Care and Use Committee. Female severe combined immunodeficient mice 8–12 wk old (CB17/lcr-*Prkdc*^{scid}, strain 561; Charles River Laboratories) were injected subcutaneously in the right shoulder with 5×10^6 Raji cells in 100 μL of phosphate-buffered saline. After about 14 d, mice with palpable tumors were injected via the tail vein with 3.7 MBq of ^{89}Zr-labeled antibody (specific activity, 222–296 MBq/mg). Small-animal PET/CT images were acquired with cross-calibrated scanners (Inveon PET/CT and Focus 220 PET) at approximately 24, 72, and 168 h after injection and coregistered. Using PET images, free-form volumetric regions of interest were drawn using Inveon Research Workstation software by an unmasked researcher, with care taken to avoid spillover from adjacent tissues. SUV_{ave} and SUV_{max} were determined for the volumetric regions of interest and calculated using the formula SUV = (MBq/mL) × animal weight (g)/injected dose (MBq) corrected for decay. For biodistribution studies, the mice were sacrificed at 168 h after injection, and organs and tissues were collected, weighed, and assayed by γ-counting. Radioactivity is expressed as the decay-corrected percentage of the injected dose per gram (%ID). If the entire tissue was not collected, for example, for bone and blood, %ID was determined using standard values for the percentage mass of that tissue. Seven mice were injected with ^{89}Zr-IgG, 5 with ^{89}Zr-obinutuzumab, 9 with ^{89}Zr-ofatumumab, 8 with ^{89}Zr-rituximab, and 4 with ^{89}Zr-tositumomab.

In Vitro Cell-Binding Studies

The immunoreactivity of ^{89}Zr-labeled anti-CD20 antibodies was determined by the assay of Lindmo and Bunn (*18,19*). Briefly, 3,000–5,000 cpm (~750 pg) of ^{89}Zr-antibody was incubated with

serial dilutions of Raji cells (starting with 5×10^5 cells) for 1 h at 23°C and then washed with phosphate-buffered saline, and the fraction of bound antibody was determined with a γ-counter. Binding in assays lacking cells was less than 5% of binding to the maximal cell amount and was subtracted.

Hematoxylin and Eosin Staining

Tumors were fixed in formalin, embedded in paraffin, sectioned, stained with hematoxylin and eosin, and examined at ×200 magnification.

Statistical Methods

Multiple comparisons were done using 1-way ANOVA with the Tukey test. A *P* value of less than 0.05 was considered statistically significant.

RESULTS

^{89}Zr-Anti-CD20 Radiochemistry, Immunoreactivity, and Stability

Initial experiments indicated that conjugation of Dfo at Dfo-to-antibody molar ratios of 10:1 and 5:1 resulted in similar specific activities after chelation with 370 kBq of ^{89}Zr/μg antibody. Because a 2:1 Dfo-to-antibody ratio resulted in an approximately 50% reduction in ^{89}Zr chelation, the 5:1 Dfo-to-antibody ratio was chosen for further studies. The radiochemical purity of all ^{89}Zr-labeled antibodies was more than 90% after diethylenetriaminepentaacetic acid competition and more than 95% after spin column purification, as assayed by instant thin-layer chromatography. By fast protein liquid chromatography, all radiolabeled antibodies showed no evidence of aggregation. ^{89}Zr-labeled obinutuzumab, ofatumumab, rituximab, and tositumomab displayed 67%, 76%, 40%, and 79% immunoreactivity, respectively, as determined by the assay of Lindmo and Bunn (*18,19*).

To assay in vitro stability, radiolabeled antibodies were incubated in human serum at 37°C or 4°C for 7 d and radiochemical purity assayed by thin-layer chromatography on days 1, 2, 3, 5, and 7. At 37°C, all antibodies retained a radiochemical purity of more than 95% up to day 5. At day 7, ofatumumab and tositumomab displayed over 98% radiochemical purity, and that of IgG, obinutuzumab, and rituximab was more than 91%. At 4°C, all antibodies displayed radiochemical purity of more than 95% at all times.

PET/CT Imaging and SUV Analyses

To evaluate in vivo targeting of ^{89}Zr-CD20 antibodies, xenograft tumors were generated in severe combined immunodeficient mice by subcutaneous injection of CD20-expressing Raji cells. Tumor-bearing mice were injected intravenously with ^{89}Zr-labeled IgG (as control) or ^{89}Zr-labeled anti-CD20 antibodies, and PET/CT images were acquired at approximately 24, 48, and 168 h after injection. At sacrifice, average tumor mass was 0.52 ± 0.22 g, with no significant difference among the groups. Staining of tumors with hematoxylin and eosin indicated no large regions of necrosis.

As seen in the PET/CT images (Fig. 1), ^{89}Zr-IgG did not show visible tumor accumulation. In contrast, obinutuzumab, ofatumumab, rituximab, and tositumomab showed clear tumor localization at all time points. Although all antibodies showed some localization to the spleen, splenic localization of ^{89}Zr-tositumomab was clearly elevated.

Volumes of interest were drawn over the heart (as a proxy for blood), kidney, liver, muscle, spine (as a proxy for bone), and tumor. SUV_{ave} and SUV_{max} for these volumes of interest were then determined, using decay-corrected values (Fig. 2). ^{89}Zr-IgG showed a consistently low tumor SUV_{ave} (Fig. 1A), as expected. IgG SUV_{ave} also was low and stable for kidney, liver, and muscle, with a modest increase in spine SUV_{ave} over time, suggesting some release of ^{89}Zr from the antibody and subsequent incorporation into bone, and with a modest decrease in heart SUV_{ave} over time, suggesting clearance from the blood or elimination from the animal.

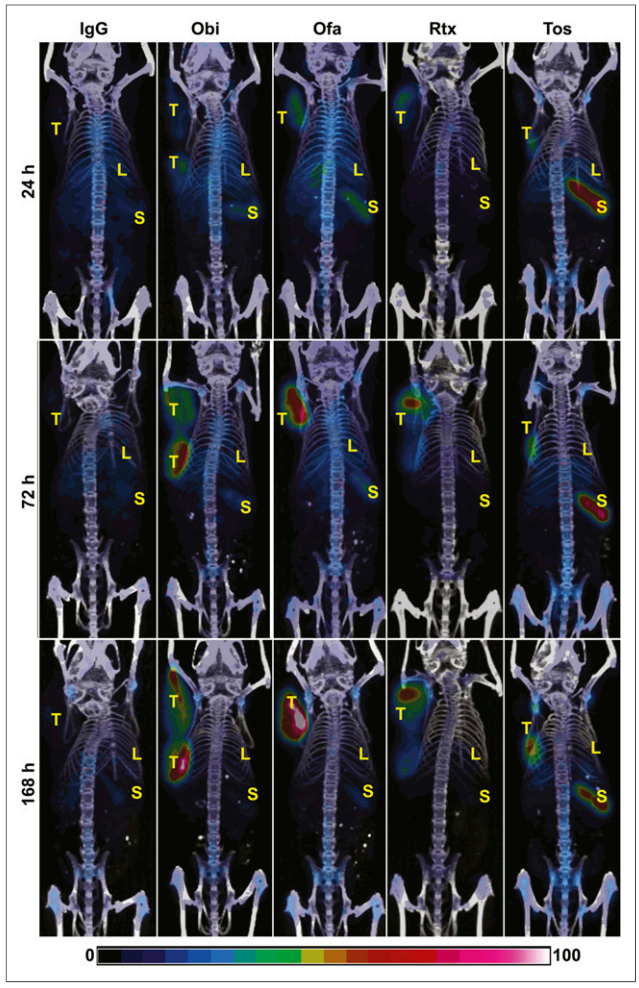

FIGURE 1. PET/CT imaging. Severe combined immunodeficient mice with Raji xenografts were injected intravenously with ^{89}Zr-IgG or ^{89}Zr-anti-CD20 antibodies, as indicated. PET/CT images were acquired at days 1, 3, and 7. Images are representative and are maximal-intensity projections corrected for decay. Bar indicates relative intensity scale. Obi = obinutuzumab; Ofa = ofatumumab; Rtx = rituximab; Tos = tositumomab; T = tumor; L = liver; S = spleen.

The anti-CD20 antibodies—^{89}Zr-obinutuzumab, ^{89}Zr-ofatumumab, ^{89}Zr rituximab, and ^{89}Zr-tositumomab—all showed a high tumor SUV_{ave} of more than 2.0 at all time points (Fig. 2A), with an increase in SUV_{ave} apparent at days 3 and 7 compared with day 1. All 4 anti-CD20 antibodies showed a slight decrease in heart SUV_{ave} and an increase in spine SUV_{ave} over the time course, as was also seen for IgG. Spine SUV_{ave} was notably higher for ^{89}Zr-tositumomab than for the other anti-CD20 antibodies. Kidney, liver, and muscle SUV_{ave} decreased during the time course for all 4 anti-CD20 antibodies.

We next directly compared tumor SUV_{ave} and SUV_{max} for the 4 anti-CD20 antibodies to IgG by ANOVA, comparing corresponding time points (Fig. 2B). At day 1, tumor SUV_{ave} for ofatumumab and rituximab was significantly higher than IgG. At day 3, all 4 anti-CD20

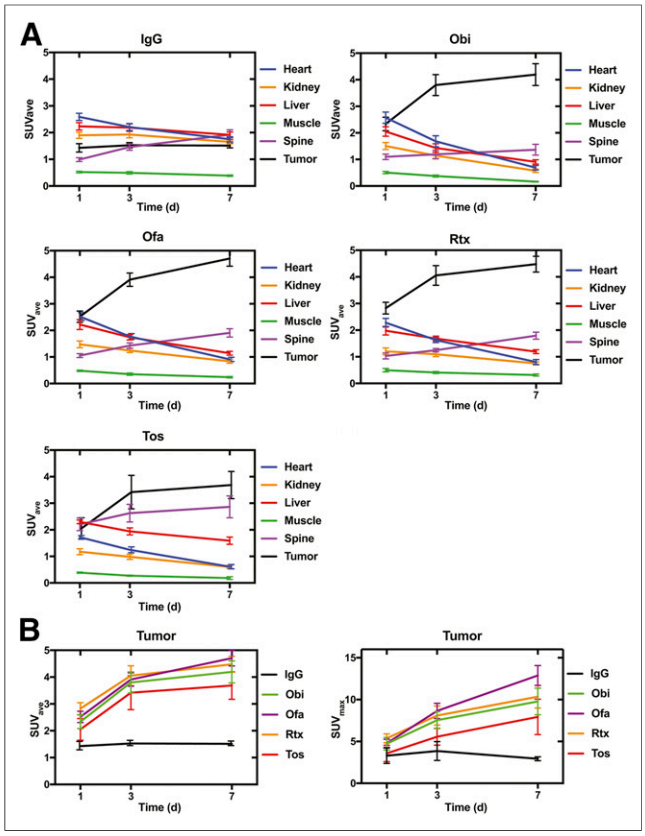

FIGURE 2. (A) SUV_{ave} time–activity curves for ^{89}Zr-labeled IgG and ^{89}Zr-anti-CD20 antibodies from PET. (B) Tumor SUV_{ave} and tumor SUV_{max} time–activity curves of ^{89}Zr-labeled antibodies. Obi = obinutuzumab; Ofa = ofatumumab; Rtx = rituximab; Tos = tositumomab. Data are mean ± SEM.

antibodies showed a significantly higher tumor SUV_{ave} than IgG. SUV_{max} tumor results were generally consistent with the SUV_{ave} findings. At day 1, no significant differences in SUV_{max} were found. At day 3, tumor SUV_{max} for ofatumumab and rituximab were significantly higher than IgG, and at day 7, tumor SUV_{max} for obinutuzumab, ofatumumab, and rituximab (but not tositumomab) were significantly higher than IgG. Although splenic uptake was visually greater for ^{89}Zr-tositumomab, isolating the spleen for SUV measurement was difficult. Together, the imaging and SUV data indicate that all 4 ^{89}Zr-anti-CD20 antibodies specifically targeted tumor, with obinutuzumab, ofatumumab, and rituximab appearing superior to tositumomab.

Biodistribution

After imaging of the mice at 168 h, biodistribution analyses were performed (Fig. 3; Table 1). As expected from the PET/CT imaging and SUV analyses, all CD20 antibodies localized well to tumor, displaying a percentage injected dose (%ID)/g of more than 27, significantly higher than that of IgG (7.2 %ID/g). Obinutuzumab yielded the highest tumor %ID/g (>41%).

For all 4 anti-CD20 antibodies, blood, heart, liver, kidney, lung, muscle, and pancreas showed a lower %ID/g than IgG. Bone showed a relatively constant %ID/g (~10) for all antibodies, and spleen was low for all except tositumomab, which was significantly higher, consistent with the PET imaging. Fat and lower-large-intestine %ID/g was similar for all antibodies, whereas stomach %ID/g tended to be lower for all CD20 antibodies. The lower large intestine was unchanged, whereas in the upper large intestine and small intestine, %ID/g tended to be lower for obinutuzumab and ofatumumab and was elevated for tositumomab. In the small intestine, obinutuzumab and ofatumumab showed a lower %ID/g than IgG whereas tositumomab was elevated.

As another way to evaluate tumor biodistribution, we determined normalized %ID/g ratios of tumor to bone, blood, liver, and muscle (Fig. 4). For tumor-to-blood, all 4 anti-CD20 antibodies showed elevated ratios, compared with IgG. Similar results were found for tumor-to-muscle, with obinutuzumab significantly outperforming ofatumumab and rituximab. For tumor-to-liver, the obinutuzumab, ofatumumab, and rituximab ratios were elevated compared with IgG, whereas the tositumomab ratios were not, with obinutuzumab outperforming rituximab. Finally, for tumor-to-bone, obinutuzumab, ofatumumab, and rituximab all showed higher ratios than did IgG or tositumomab, with obinutuzumab outperforming rituximab.

DISCUSSION

Anti-CD20 immunotherapy and, to a lesser extent, anti-CD20 radioimmunotherapy have revolutionized treatment of NHL and other hematologic malignancies. In July of 2017, obinutuzumab was recommended by the National Institute for Health and Care Excellence as a combination treatment with chemotherapy for patients with follicular lymphoma who have not responded to rituximab-based treatment and as monotherapy for maintenance thereafter. Here, we present the generation and preclinical characterization of

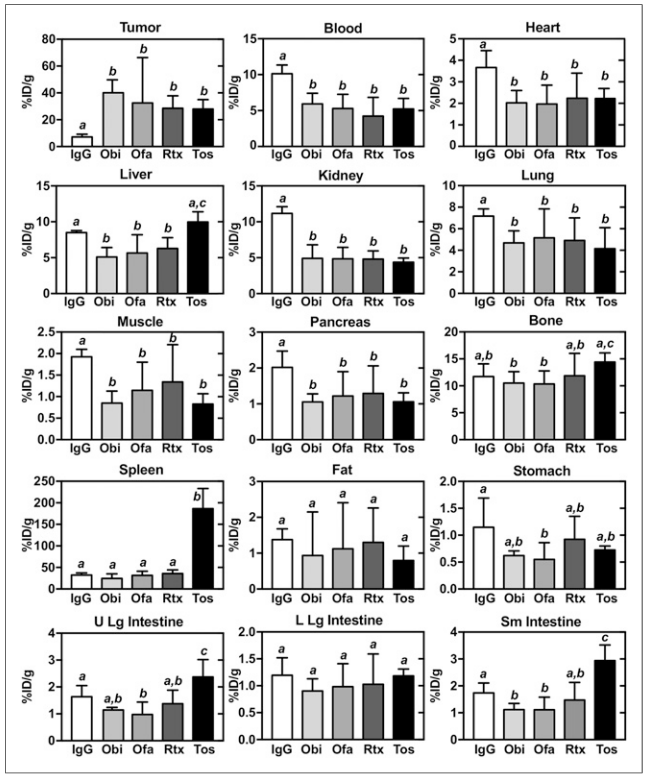

FIGURE 3. Organ and tissue biodistribution of ^{89}Zr-IgG and ^{89}Zr-anti-CD20 antibodies at day 7 in mice with Raji xenografts. Obi = obinutuzumab; Ofa = ofatumumab; Rtx = rituximab; Tos = tositumomab. Data are mean ± SD. Differences between uptake levels are present at $P < 0.05$ if there is no shared italicized letter, as analyzed by 1-way ANOVA with Tukey test.

TABLE 1
Biodistribution of ^{89}Zr-Labeled Anti-CD20 Antibodies and ^{89}Zr-IgG

Tissue	Obinutuzumab (n = 5)	Ofatumumab (n = 9)	Rituximab (n = 8)	Tositumomab (n = 4)	IgG (n = 7)
Tumor	41.44 ± 7.56	32.56 ± 17.48	28.62 ± 7.60	27.95 ± 6.45	7.20 ± 1.24
Liver	5.10 ± 0.98	5.65 ± 1.27	6.29 ± 1.11	9.99 ± 1.03	8.50 ± 0.21
Spleen	24.59 ± 9.12	31.82 ± 7.28	36.01 ± 7.58	186.39 ± 49.69	32.51 ± 3.76
Blood	5.92 ± 1.62	5.29 ± 1.66	4.24 ± 1.80	5.23 ± 1.35	10.14 ± 0.86
Bone	10.51 ± 1.22	10.34 ± 1.36	11.87 ± 2.05	14.42 ± 2.03	11.72 ± 1.58
Muscle	0.85 ± 0.18	1.15 ± 0.43	1.34 ± 0.53	0.83 ± 0.22	1.93 ± 0.15
Upper large intestine	1.14 ± 0.16	0.97 ± 0.32	1.38 ± 0.32	2.37 ± 0.48	1.64 ± 0.39
Lower large intestine	0.90 ± 0.25	0.98 ± 0.25	1.03 ± 0.36	1.18 ± 0.15	1.20 ± 0.28
Small intestine	1.12 ± 0.18	1.11 ± 0.31	1.48 ± 0.47	2.94 ± 0.42	1.74 ± 0.30
Kidney	4.90 ± 1.08	4.85 ± 1.14	4.80 ± 0.93	4.38 ± 0.42	11.16 ± 0.79
Heart	2.02 ± 0.37	1.97 ± 0.53	2.23 ± 0.84	2.22 ± 0.49	3.67 ± 0.53
Pancreas	1.05 ± 0.20	1.22 ± 0.36	1.29 ± 0.36	1.06 ± 0.19	2.02 ± 0.31
Stomach	0.62 ± 0.12	0.55 ± 0.20	0.92 ± 0.42	0.73 ± 01.11	1.15 ± 0.46
Lung	4.68 ± 0.90	5.16 ± 1.49	4.91 ± 1.45	4.15 ± 1.37	7.18 ± 0.68

Data are mean ± SD %ID/g.

^{89}Zr-obinutuzumab (humanized), ofatumumab (fully human), rituximab (mouse/human chimera), and tositumomab (mouse) antibodies. In ^{89}Zr-immuno-PET and biodistribution studies using human lymphoma xenografts in mice, we found that for specific tumor targeting, obinutuzumab and ofatumumab performed as well as, or superior to, rituximab and tositumomab, with all anti-CD20 antibodies being superior to control IgG. Thus, both ^{89}Zr-obinituzimab and ^{89}Zr-ofatumumab show potential for clinical use in immuno-PET for monitoring treatment efficacy and, more probably, as components of theranostics for radioimmunotherapy regimens.

In this study, we chose Dfo-^{89}Zr as the chelator-tracer combination. Among the available chelators for ^{89}Zr, Dfo is commercially available in good-manufacturing-practice grade and requires simple chemistry for antibody conjugation. Dfo-conjugated antibodies generally retain high biologic activity, and antibodies chelated to ^{89}Zr via Dfo typically show acceptably low rates of demetallation in vivo. In addition, ^{89}Zr is relatively inexpensive, is widely available, has a half-life (3.3 d) appropriate for clearance of nonspecifically bound antibodies in vivo, and has excellent characteristics for PET imaging (*20*). Because of these qualities, multiple ^{89}Zr-Df-antibody immuno-PET tracers are currently in use in multiple clinical trials. Indeed, human use of ^{89}Zr-rituximab was reported recently in lymphoma patients (*20,21*).

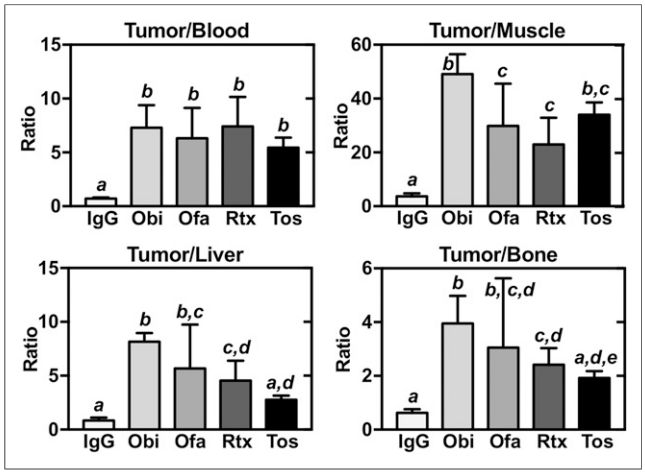

FIGURE 4. Tumor biodistribution of ^{89}Zr-IgG and ^{89}Zr-anti-CD20 antibodies at day 7 in mice with Raji xenografts, normalized to blood, muscle, liver, or bone. Obi = obinutuzumab; Ofa = ofatumumab; Rtx = rituximab; Tos = tositumomab. Data are mean ± SD. Differences between normalized uptake levels are present at $P < 0.05$ if there is no shared italicized letter, as analyzed by 1-way ANOVA with Tukey test.

One concern for ^{89}Zr-immuno-PET is demetallation of the ^{89}Zr-antibody and incorporation of ^{89}Zr into bone or other tissues. We found that all ^{89}Zr-anti-CD20 antibodies showed acceptable stability in vitro, with more than 90% radiochemical purity after 7 d at 37°C in human serum. By quantitative immuno-PET and biodistribution analyses, we found that the SUV_{ave} for spine was approximately 1 for all anti-CD20 antibodies except tositumomab (SUV_{ave}, ~2) and increased by approximately only 2-fold over the 7-d time course. Biodistribution confirmed a relatively low bone %ID/g of 10–15 at day 7. Thus, ^{89}Zr chelation by the Dfo-conjugated anti-CD20 antibodies appears reasonably stable in vivo over an extended period.

Tumor targeting was efficient, and generally comparable, among ^{89}Zr-obinutuzumab, ^{89}Zr-ofatumumab, and ^{89}Zr-rituximab, as assayed by SUV_{ave} and SUV_{max}, with obinutuzumab and ofatumumab performing at least as well as rituximab. ^{89}Zr-tositumomab tumor targeting was comparable to the other agents, but ^{89}Zr-tositumomab displayed relatively high bone and spleen localization. Tumor biodistribution, without or with normalization to bone, blood, liver, or muscle, reinforced these findings. Together, the results indicate that ^{89}Zr-obinutuzumab, ^{89}Zr-ofatumumab, and ^{89}Zr-rituximab performed well, with obinutuzumab tending to perform somewhat better for tumor targeting and specificity.

In blood, kidney, and liver, SUV_{ave} and biodistribution analyses indicated a continual decline in tracer uptake in these nontarget tissues with the ^{89}Zr-anti-CD20 antibodies, but not with ^{89}Zr-IgG, over the 7-d time course. One potential explanation is clearance of

antibodies from the animal. However, incorporation of the ^{89}Zr-CD20 antibodies into tumor continually increased over the time course, showing an approximately 2-fold increase at day 3 and a further increase at day 7, probably contributing to a portion of the clearance from the blood. A notable finding was the high incorporation of radiolabeled tositumomab in the spleen, as shown by PET imaging and biodistribution analysis. One possibility is that the spleen is an effective sink for this antibody, particularly as it is the only fully-mouse antibody used in the study. Prior studies with ^{131}I-tositumomab in a similar animal model showed high splenic uptake, which was protein-mass–dependent (*22*).

^{89}Zr anti-CD20 antibodies have potential for both the prognostic evaluation of NHL and the monitoring of treatment. The more lymphoma-specific binding of ^{89}Zr anti-CD20 antibodies may offer advantages over ^{18}F-FDG, which can accumulate in both tumor and inflammatory infiltrates. Although the Fc of the intact antibody may bind to Fc receptors on inflammatory cells, this could be mitigated, if problematic, through the use of antibody fragments or engineered high-affinity variants with no or modified Fc regions (*23,24*). Further, some forms of NHL show low ^{18}F-FDG avidity, for example, mucosa-associated lymphoid tissue marginal zone lymphoma, small lymphocytic lymphoma, and others (*20*). ^{89}Zr-PET has the potential advantage of using the high avidity and affinity of anti-CD20 antibodies to detect lymphoma cells in vivo, allowing for improved diagnosis and evaluation of treatment response (*20*).

A few previous studies have evaluated the potential for anti-CD20 antibodies in PET studies of NHL. Natarajan et al. have generated ^{89}Zr-rituximab and evaluated its use in a humanized CD20 mouse model (*21*). A small number of humans with NHL were studied with this agent, as well, with findings suggesting substantial opportunities for refining patient dosimetry (*25,26*). Our findings suggest that next-generation human and humanized anti-CD20 antibodies have excellent potential as imaging agents and as part of a theranostic regimen for NHL and other B-cell proliferations.

CONCLUSION

We have developed next-generation anti-CD20 antibodies using ^{89}Zr for PET identification and evaluation of CD20-expressing tumor cells in vivo. PET imaging with these reagents may be useful in diagnosis and treatment evaluation of patients with lymphoma, as well as having potential for radioimmunotherapy with repeated dosing.

DISCLOSURE

This study was funded, in part, by a Radiological Society of North America Education and Research Foundation Medical Student research award, RMS1646, to Jason Yoon and Richard Wahl. Bernadette Marquez-Nostra is supported by the National Institutes of Health (grant 1K99CA201601). No other potential conflict of interest relevant to this article was reported.

ACKNOWLEDGMENTS

We appreciate the assistance provided by the Washington University Small Animal Imaging Core and the cyclotron facilities.

REFERENCES

1. Cancer stat facts: non-Hodgkin lymphoma. National Cancer Institute Surveillance, Epidemiology, and End Results Program website. http://seer.cancer.gov/statfacts/html/nhl.html. Accessed April 27, 2018.
2. Ku M, Chong G, Hawkes EA. Tumour cell surface antigen targeted therapies in B-cell lymphomas: beyond rituximab. *Blood Rev.* 2017;31:23–35.
3. Polito L, Bortolotti M, Maiello S, Battelli MG, Bolognesi A. Rituximab and other new anti-CD20 mabs for non-Hodgkin's lymphoma treatment. *EMJ Oncol.* 2014;2:63–69.
4. Kaminski MS, Zasadny KR, Francis IR, et al. Radioimmunotherapy of B-cell lymphoma with [^{131}I]anti-B1 (anti-CD20) antibody. *N Engl J Med.* 1993;329:459–465.
5. Kaminski MS, Tuck M, Estes J, et al. ^{131}I-tositumomab therapy as initial treatment for follicular lymphoma. *N Engl J Med.* 2005;352:441–449.
6. Kaminski MS, Radford JA, Gregory SA, et al. Re-treatment with I-131 tositumomab in patients with non-Hodgkin's lymphoma who had previously responded to I-131 tositumomab. *J Clin Oncol.* 2005;23:7985–7993.
7. Kaminski MS, Estes J, Zasadny KR, et al. Radioimmunotherapy with iodine ^{131}I tositumomab for relapsed or refractory B-cell non-Hodgkin lymphoma: updated results and long-term follow-up of the University of Michigan experience. *Blood.* 2000;96:1259–1266.
8. Zevalin (ibritumomab tiuxetan) full prescribing information. U.S. Food and Drug Administration website. http://www.accessdata.fda.gov/drugsatfda_docs/label/2013/125019s210s213lbl.pdf.Revised August 2013. Access April 27, 2018.
9. Bexxar (tositumomab and iodine I 131 tositumomab) full prescribing information. U.S. Food and Drug Administration website. https://www.accessdata.fda.gov/drugsatfda_docs/label/2012/125011s102lbl.pdf. Revised February 2012. Accessed April 27, 2018.
10. Kesavan M, Boucek J, MacDonald W, McQuillan A, Turner JH. Imaging of early response to predict prognosis in the first-line management of follicular non-Hodgkin lymphoma with iodine-131-rituximab radioimmunotherapy. *Diagnostics (Basel).* 2017;7:e26.
11. Klein C, Lammens A, Schafer W, et al. Epitope interactions of monoclonal antibodies targeting CD20 and their relationship to functional properties. *MAbs.* 2013;5:22–33.
12. Gazyva (obinutuzumab) full prescribing information. U.S. Food and Drug Administration website. http://www.accessdata.fda.gov/drugsatfda_docs/label/2017/125486s017s018lbl.pdf. Revised November 2017. Accessed April 27, 2018.
13. Arzerra (ofatumumab) full prescribing information. U.S. Food and Drug Administration website. http://www.accessdata.fda.gov/drugsatfda_docs/label/2009/125326lbl.pdf. Revised October 2009. Accessed April 27, 2018.
14. Baldo BA. Adverse events to monoclonal antibodies used for cancer therapy: focus on hypersensitivity responses. *Oncoimmunology.* 2013;2:e26333.
15. Barth MJ, Mavis C, Czuczman MS, Hernandez-Ilizaliturri FJ. Ofatumumab exhibits enhanced *in vitro* and *in vivo* activity compared to rituximab in preclinical models of mantle cell lymphoma. *Clin Cancer Res.* 2015;21:4391–4397.
16. Mössner E, Brunker P, Moser S, et al. Increasing the efficacy of CD20 antibody therapy through the engineering of a new type II anti-CD20 antibody with enhanced direct and immune effector cell-mediated B-cell cytotoxicity. *Blood.* 2010;115:4393–4402.
17. Laforest R, Lapi SE, Oyama R, et al. [^{89}Zr]trastuzumab: evaluation of radiation dosimetry, safety, and optimal imaging parameters in women with HER2-positive breast cancer. *Mol Imaging Biol.* 2016;18:952–959.
18. Marquez BV, Ikotun OF, Zheleznyak A, et al. Evaluation of ^{89}Zr-pertuzumab in breast cancer xenografts. *Mol Pharm.* 2014;11:3988–3995.
19. Lindmo T, Bunn PA. Determination of the immunoreactive function of radiolabeled monoclonal antibodies by linear extrapolation to binding at infinite antigen excess. *J Immunol Methods.* 1984;72:77–89.
20. England CG, Rui L, Cai W. Lymphoma: current status of clinical and preclinical imaging with radiolabeled antibodies. *Eur J Nucl Med Mol Imaging.* 2017;44:517–532.
21. Natarajan A, Habte F, Gambhir SS. Development of a novel long-lived immunoPET tracer for monitoring lymphoma therapy in a humanized transgenic mouse model. *Bioconjug Chem.* 2012;23:1221–1229.
22. Buchsbaum DJ, Wahl RL, Glenn SD, Normolle DP, Kaminski MS. Improved delivery of radiolabeled anti-B1 monoclonal antibody to Raji lymphoma xenografts by predosing with unlabeled anti-B1 monoclonal antibody. *Cancer Res.* 1992;52:637–642.
23. Maute RL, Gordon SR, Mayer AT, et al. Engineering high-affinity PD-1 variants for optimized immunotherapy and immuno-PET imaging. *Proc Natl Acad Sci USA.* 2015;112:E6506–E6514.
24. Saxena A, Wu D. Advances in therapeutic Fc engineering: modulation of IgG-associated effector functions and serum half-life. *Front Immunol.* 2016;7:580.
25. Jauw YW, Zijlstra JM, de Jong D, et al. Performance of ^{89}Zr-labeled-rituximab-PET as an imaging biomarker to assess CD20 targeting: a pilot study in patients with relapsed/refractory diffuse large B cell lymphoma. *PLoS One.* 2017;12:e0169828.
26. Muylle K, Flamen P, Vugts DJ, et al. Tumour targeting and radiation dose of radioimmunotherapy with ^{90}Y-rituximab in CD20+ B-cell lymphoma as predicted by ^{89}Zr-rituximab immuno-PET: impact of preloading with unlabelled rituximab. *Eur J Nucl Med Mol Imaging.* 2015;42:1304–1314.